In Situ Investigation of Degradation at Organometal Halide Perovskite Surfaces by X-ray Photoelectron Spectroscopy in Realistic Water Atmospheres

Chun-Ren Ke, Alex S. Walton, David J. Lewis, Aleksander Tedstone, Paul O'Brien, Andrew G. Thomas,* and Wendy R. Flavell*

Electronic Supplementary Information†

Experimental details

Preparation of methylammonium iodide (MAI)

MAI was prepared as follows: 38 mL methylamine (CH_3NH_2, MA) solution (Aldrich, 33 wt% in absolute ethanol) was added dropwise to 40 mL hydroiodic (HI) acid solution (Sigma-Aldrich, 57 wt% in H_2O). The solution was stirred for 1 hour whilst maintaining the reaction temperature at ~0 - 10 °C by use of an ice bath. The solution was subsequently allowed to warm to room temperature. Solvent was removed by a rotary evaporator in a water bath at 60 to 90 °C. Approximately 45 g of white, crystalline methylammonium iodide (CH_3NH_3I, MAI) powder was obtained after drying in a vacuum oven overnight.

Perovskite thin film preparation

Perovskite thin films were deposited *via* an *in situ* thermal evaporator integrated into the NAPXPS system. $PbCl_2$ (Aldrich, 98%) and the synthesised MAI were placed in a simple dual source Knudsen cell, each with a thermocouple attached in order to measure the evaporation temperatures. $PbCl_2$ and MAI were evaporated at temperatures of 400 °C and 160 °C, respectively onto a $SrTiO_3$ (100) single crystal substrate (MTI Corp.) held at a distance of around 2 cm from the Knudsen cell. Prior to the deposition, the $SrTiO_3$ substrate was heated to approximately 600 °C to remove the surface contaminants and to increase the conductivity.[1]

$PbCl_2$ and MAI were simultaneously evaporated onto the substrate for the first 10 minutes. After 10 minutes, the current to the $PbCl_2$ was shut off, whilst continuing to heat the MAI for a further 20 minutes until chlorine was no longer observed in the XPS spectrum as shown in Fig. S1 below. Prior to XPS measurements, the deposited film was post-annealed at 50 °C for 10 minutes in *vacuo* to ensure formation of the perovskite structure; however we note that several reports have indicated that post-annealing is not necessary for samples fabricated *via* vapour deposition.[2-4] Use of higher annealing temperatures led to thermal decomposition/desorption of the film under UHV conditions. This procedure led to growth of a film of composition consistent with the expected stoichiometry of the methylammonium lead iodide (MAPI) film (see main text). These film growth conditions were optimised to produce a few-nm-thick film, sufficiently thin to be entirely probed by the XPS experiment, as described further below. This was necessary to add confidence to the quantification of sample stoichiometry from XPS. The stoichiometry of the film, together with the absence of signals from $PbCl_2$ in XPS (see below) were taken to indicate complete reaction of the $PbCl_2$ with the MAI to form a methylammonium lead iodide film. This material was then transferred in UHV into the near ambient pressure (NAP) cell.

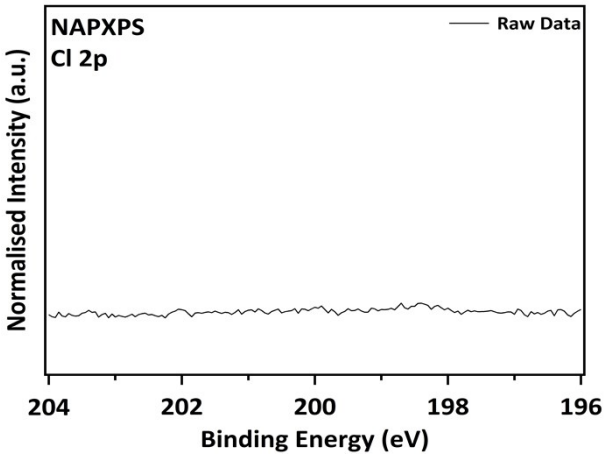

Fig. S1 XPS spectrum of the Cl 2p core level region of the MAPI perovskite film (UHV before water exposure). The intensity is normalised to the Sr $3d_{5/2}$ signal of the substrate (*i.e.* the data are normalised in the same way as in Fig. 1 of the main text). It is clear that no detectable chlorine remains on the surface of the film following reaction of $PbCl_2$ with MAI to form the MAPI film.

X-ray Diffraction

X-ray diffraction (XRD) was carried out on a separate thin film grown in UHV by the same method as that studied by Near-Ambient Pressure X-Ray Photoelectron Spectroscopy (NAPXPS) in order to confirm that the vacuum-deposited films did indeed have the perovskite structure. It was necessary to carry out this measurement on a separate film, as the aim of our experiment was to study the degradation of a pristine film (which had not been exposed to air) by NAPXPS; the film at the end of the experiment is no longer MAPI.

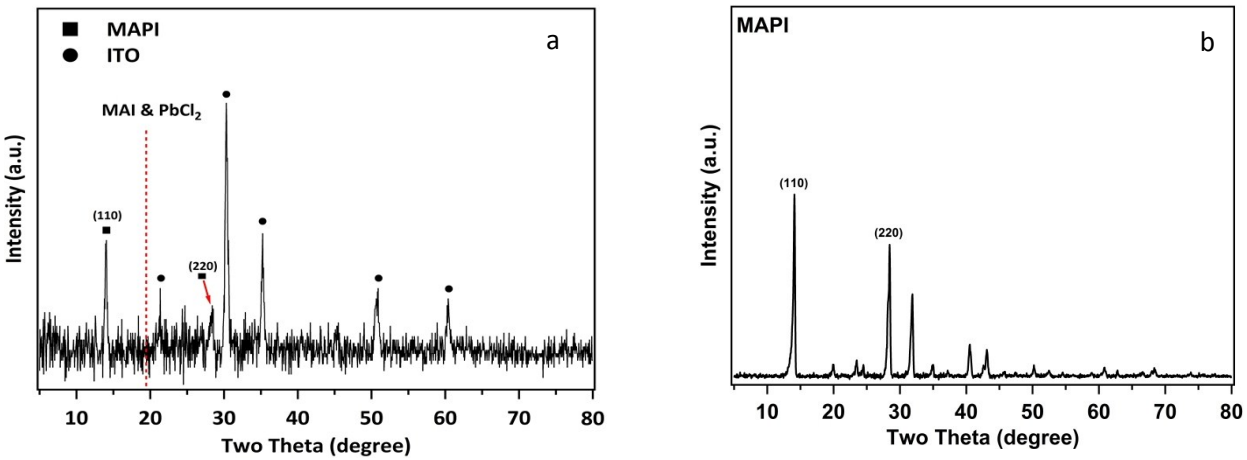

Fig. S2 **a)** X-Ray diffraction pattern of the vacuum-deposited perovskite thin film on an ITO-coated glass slide. Squares mark diffraction peaks associated with the MAPI film and the circles the reflections due to the underlying ITO. b) XRD from bulk MAPI perovskite film grown by aerosol-assisted chemical vapour deposition. The dashed line in a) indicates the position of the primary diffraction peaks of MAI and $PbCl_2$ at 19.5° and 19.6° respectively, demonstrating no precursor-phase remnants in the MAPI film.[5, 6]

XRD was carried out using a Bruker D8 Advance instrument, with the capability for grazing incidence measurements, necessary for the acquisition of diffraction information from the few-nm-thick film. An X-ray grazing incidence angle of 3° was used to detect the signals from the thin films over a range (2θ) of 5° to 80° with a step size of 0.05° and dwell time of 4.5 seconds per point. The diffractogram of the as-deposited film is shown in Fig. S2a), and clearly shows diffraction peaks due to MAPI. The preferred orientation of the (110) planes is in agreement with XRD from a bulk MAPI film grown *ex situ* by a vapour-deposition route (aerosol-assisted chemical vapour deposition) (Figure S2b) and with previous work using solution based deposition techniques[7]. The thin film was grown on tin-doped indium oxide (ITO) glass using a total deposition time of three times that used for the NAPXPS film described below, giving an estimated film thickness of *ca.* 6 nm. From the X-ray absorption coefficient of MAPI (25.884 mm^{-1} [8]), and the incidence angle of 3 degrees, we calculate the X-ray penetration depth to be ~2 μm. Thus as expected the XRD pattern is dominated by reflections from the ITO substrate. We also note that no intensity is observed at a 2θ value corresponding to the primary reflections of the $PbCl_2$ and MAI precursors (shown by the red dashed line in figure S2a).

NAPXPS measurements

The NAPXPS apparatus used in this work is equipped with a SPECS Focus 500 monochromated Al Kα source with photon energy of 1486.6 eV. The analyser for NAP is a SPEC 150 mm Phoibos 150 NAP fitted with a three-stage, differentially pumped electrostatic lens. XPS measurements can be carried out under the conventional conditions in the UHV chamber as well in a near ambient pressure cell which couples to the entrance cone of the analyser lens system. For the NAP measurements, the cell was backfilled with H_2O vapour to reach pressures of 3 mbar and 9 mbar, which roughly corresponds to relative humidity (RH) of 10% and 30%, respectively, under a standard atmospheric temperature of 25 °C. The water was purified by repeated freeze-thaw cycles.

The binding energy (BE) was calibrated to well-defined Sr $3d_{5/2}$ peak at 133.70 eV, which arises from the $SrTiO_3$ substrate.[9-11] This gives a Ti $2p_{3/2}$ binding energy of 459.20 eV, in good agreement with the value for Ti^{4+} measured by the same equipment previously.[12] BE values are quoted to an accuracy of ±0.05 eV, and thus a binding energy shift of 0.2 eV can be clearly observed. A Shirley background was subtracted from the data presented in the manuscript and supporting information.[13] GL(30) function (70% Gaussian and 30% Lorentzian) curves were used to fit the core level spectra using CasaXPS software.[14] The built in CASAXPS sensitivity factors are used for calculating the stoichiometry of the sample before and after water exposure from UHV measurements only, since transmission-function-adapted data do not currently exist for near-ambient pressure conditions. These sensitivity factors include a correction for the escape depth of the photoelectrons.

In order to add confidence to the quantification of the XPS data, a very thin (few-nm-thick) film was grown for the experiment, where the core level signals due to the underlying substrate remained visible in XPS after film deposition. These were used in the quantification as described below. A calculation of the film thickness using a two-layer model based on a MAPI film grown on the $SrTiO_3$ substrate can be made using equation S1:

$$\frac{I_{Pb}}{I_{Sr}} = \frac{N_{Pb}\sigma_{Pb}\lambda_{Pb}}{N_{Sr}\sigma_{Sr}\lambda_{Sr}}\left(\frac{1-exp\{-d/\lambda_{Pb}\}}{exp\{-d/\lambda_{Sr}\}}\right).$$

equation S1

Using the intensities (I_{Pb} and I_{Sr}) from the Pb 4f and Sr 3d peaks, with photoionisation cross sections σ_{Pb} *and* σ_{Sr}, number densities N_{Pb} *and* N_{Sr} and calculated inelastic mean free path lengths (from the NIST electron mean free path database[15]) $\lambda_{Pb} = \lambda_{Sr}$, we obtain a value for the MAPI film of 1.9 ± 1 nm. This calculation assumes that the film is of a uniform thickness with no gaps, but measurements at different points on the film revealed a uniform stoichiometry, suggesting that this is the case (see Figure S3).

With regards to the stoichiometry calculation, the use of Sr 3d and 3p peaks allows a self-check of the stoichiometry calculations, since the Pb 4f peaks appear close in binding energy to Sr 3d and the C 1s signal is close to Sr 3p, so any residual effects associated with different probe depths can be confidently accounted for. In addition, the observation of the Sr peaks through the thin film confirms we probe the whole film, thus it is unlikely that (for example) unreacted $PbCl_2$ is present beneath the MAI film, as no Cl 2p signal is present (figure S1). XPS was performed on standard samples of the $PbCl_2$ precursor. We were able to clearly resolve a binding energy shift of 0.3 eV between the Pb 4f features of MAPI and $PbCl_2$ (figure S4), adding confidence to our conclusion that a complete reaction of $PbCl_2$ with MAI to form a methylammonium lead iodide film was achieved. The stoichiometry of the resulting film was in good agreement with the nominal stoichiometry of MAPI (see main manuscript text).

Table S1 Elemental (Sr, Pb, I, N, C, and Cl) quantification of the film determined from UHV XPS at different stages, before and after water exposure. All values are normalised to the area of the Sr 3d peak in the substrate. Only the Pb^{2+} components in the film are shown in the Pb column (the Pb(0) component (main text Fig. 1, and SI Fig. S3) is excluded). We note that metallic lead is always present in the MAPI film, which is also a common phenomenon for solution-grown films processed through sequential steps as reported in the literature.[16, 17] The excess C is assumed to arise from hydrocarbon contamination, most likely outgassing from the hot Knudsen cells, but possibly also due to a small amount of dissociation of MAI in the Knudsen cell.

Sample status	Sr	Pb(II)	I	N	C	Cl
UHV before water exposure	1.00 ± 0.05	0.30 ± 0.05	0.80 ± 0.05	0.27 ± 0.1	2.40 ± 0.1	0.00 ± 0.05
UHV after water exposure	1.00 ± 0.05	0.08 ± 0.05	0.20 ± 0.05	0.00 ± 0.1	2.50 ± 0.1	0.00 ± 0.05

Table S2 Detailed quantification of the C 1s and N 1s spectra where C_A is attributed to C-H, C-I or C-C and C_B is ascribed to C-N and 'C-O' (species such as C=O/C-OH). Areas here are normalised to Sr $3d_{5/2}$ peak areas. It is clear the total C content of the film is unchanged by water exposure and that the peak corresponding to C-N and C-O species decreases in intensity by an amount consistent with the loss of N from the film. At the same time, there is a matching increase in the intensity of the C_A feature, suggesting an increase in hydrocarbon content, consistent with equation 1 of the main manuscript. The high vapour pressure of CH_3NH_3I means that a decomposition mechanism such as that shown in equation 2 of the main manuscript would result in

evaporation of this molecule under vacuum conditions. This would lead to a reduction in intensity of *both* C_A and the C-N related peak (C_B). The increase in the intensity of the C-C related peak observed here is inconsistent with this.

Sample Status	Total C	C_A (CC,CI,CH)	C_B (CN,CO)	N
UHV before water exposure	2.4 ± 0.1	1.5 ± 0.05	0.9 ± 0.1	0.27 ± 0.1
UHV after water exposure	2.5 ± 0.1	1.9 ± 0.05	0.6 ± 0.1	0.0 ± 0.1

Table S3 Quantification of Pb peak area normalised to Sr $3d_{5/2}$ peak area

Sample Status	Total Pb	Pb(II)	Pb(0)
UHV before water exposure	0.35 ± 0.05	0.30 ± 0.05	0.05 ± 0.02
UHV after water exposure	0.18 ± 0.05	0.08 ± 0.05	0.1 ± 0.05

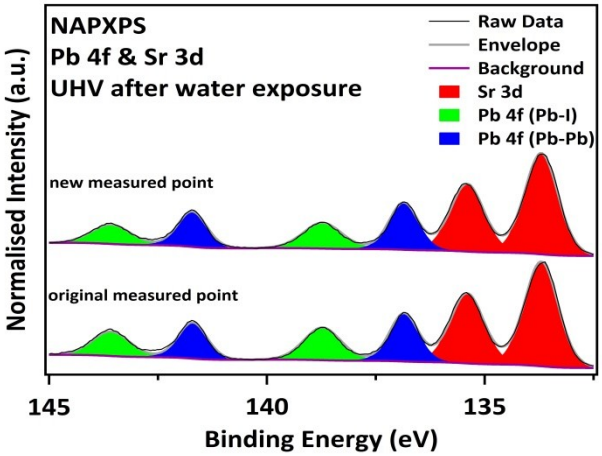

Fig. S3 XPS spectra of Pb 4f & Sr 3d core levels of the film (in UHV after water exposure) taken at two different positions (one exposed to the X-ray beam during data taking for the whole experiment, and a fresh sample position). Both points show a similar Pb(0)/Pb(II) ratio of approximately 1.2. This suggests that changes observed in the spectra are predominantly associated with water exposure rather than beam damage.

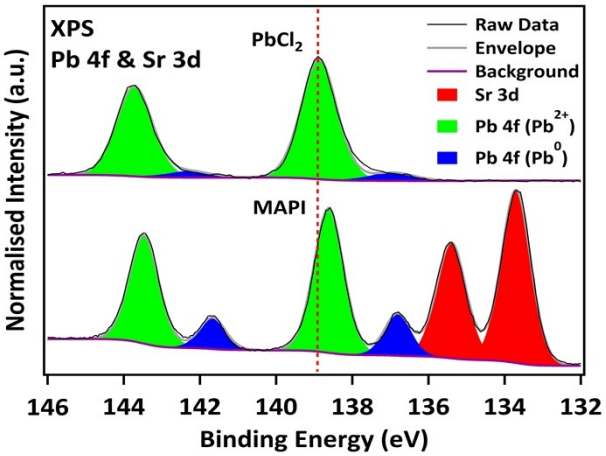

Fig. S4 a) Comparison of the Pb 4f-core-level XPS spectra of $PbCl_2$ and MAPI film showing a shift in Pb $4f_{7/2}$ BE of 0.3 eV between Pb-Cl (138.90 eV[18]) and Pb-I in MAPI (138.60 eV). The $PbCl_2$ film also contains a trace amount of metallic lead, indicating partial decomposition of vapourised $PbCl_2$.

References

1. K. Szot, W. Speier, G. Bihlmayer and R. Waser, *Nature materials*, 2006, **5**, 312-320.
2. O. Malinkiewicz, A. Yella, Y. H. Lee, G. M. Espallargas, M. Graetzel, M. K. Nazeeruddin and H. J. Bolink, *Nature Photonics*, 2014, **8**, 128-132.
3. D. Zhao, W. Ke, C. R. Grice, A. J. Cimaroli, X. Tan, M. Yang, R. W. Collins, H. Zhang, K. Zhu and Y. Yan, *Nano Energy*, 2016, **19**, 88-97.
4. J. B. Patel, J. Wong-Leung, S. Van Reenen, N. Sakai, J. T. W. Wang, E. S. Parrott, M. Liu, H. J. Snaith, L. M. Herz and M. B. Johnston, *Advanced Electronic Materials*, 2016.
5. C. Gao, J. Liu, C. Liao, Q. Ye, Y. Zhang, X. He, X. Guo, J. Mei and W. Lau, *RSC Advances*, 2015, **5**, 26175-26180.
6. N. J. Jeon, J. H. Noh, Y. C. Kim, W. S. Yang, S. Ryu and S. I. Seok, *Nature materials*, 2014, **13**, 897-903.
7. L. J. Phillips, A. M. Rashed, R. E. Treharne, J. Kay, P. Yates, I. Z. Mitrovic, A. Weerakkody, S. Hall and K. Durose, *Solar Energy Materials and Solar Cells*, 2016, **147**, 327-333.
8. C. C. Stoumpos, C. D. Malliakas and M. G. Kanatzidis, *Inorganic chemistry*, 2013, **52**, 9019-9038.
9. Y.-F. Zhu, L. Xu, J. Hu, J. Zhang, R.-G. Du and C.-J. Lin, *Electrochimica Acta*, 2014, **121**, 361-368.
10. D. M. Hill, H. Meyer III and J. Weaver, *Journal of Applied Physics*, 1989, **65**, 4943-4950.
11. W.-D. Yang, *Journal of materials science*, 1999, **34**, 3533-3544.
12. M. J. Jackman, A. G. Thomas and C. Muryn, *The Journal of Physical Chemistry C*, 2015, **119**, 13682-13690.
13. D. A. Shirley, *Physical Review B*, 1972, **5**, 4709.
14. N. Fairley, *CasaXPS manual 2.3. 15*, Acolyte Science, 2009.
15. C. Powell and A. Jablonski, *Electron Effective-Attenuation-Length, Version*, 2011, **1**.
16. W. Zhang, S. Pathak, N. Sakai, T. Stergiopoulos, P. K. Nayak, N. K. Noel, A. A. Haghighirad, V. M. Burlakov, A. Sadhanala and W. Li, *Nature communications*, 2015, **6**.
17. D. Bi, C. Yi, J. Luo, J.-D. Décoppet, F. Zhang, S. M. Zakeeruddin, X. Li, A. Hagfeldt and M. Grätzel, *Nature Energy*, 2016, **1**, 16142.

18. J.-K. Jung and W.-J. Lee, *Japanese Journal of Applied Physics*, 2001, **40**, 1408.